Hybrid Organic–Inorganic Conductor Coupled with BEDT-TTF and Photochromic Nitrosyl Ruthenium Complex

Masashi Okubo, Masaya Enomoto, Kazuko Koyama,[1] Yoshiya Uwatoko,[1] and Norimichi Kojima*

Graduate School of Arts and Sciences, The University of Tokyo, Komaba 3-8-1, Meguro-ku, Tokyo 153-8902

[1]Institute for Solid State Physics, The University of Tokyo, Kashiwa, Chiba 277-8581

Received December 6, 2004; E-mail: cnori@mail.ecc.u-tokyo.ac.jp

An organic–inorganic hybrid system coupled with an organic conductor and photosensitive transition metal complex has a possibility to exhibit fascinating multifunctionalities, such as photo-controllable conductor. To explore multifunctional materials, such as a photo-tunable conductor, we prepared $(BEDT\text{-}TTF)_4[RuCl_5(NO)]\cdot C_6H_5CN$ (BEDT-TTF: 4,5-bis(ethylenedithio)tetrathiafulvene) by electrocrystallization, and investigated the structural and physical properties. X-ray crystallographic analysis shows alternate layers of BEDT-TTF cations and ruthenium complex anions. The organic layer is formed by the dimers of BEDT-TTF arranged almost perpendicular to each other, which indicates that the donor arrangement of this salt belongs to κ-type. Based on the Raman spectrum, the oxidation state of the BEDT-TTF molecules is estimated to be +0.7. X-ray structural analysis and the EPR spectra suggest that there is a partial electron transfer from BEDT-TTF to the π^* orbital of NO ligand in $[RuCl_5(NO)]$ through a short intermolecular contact. A magnetic susceptibility measurement and the EPR spectra proved this compound to be a localized spin system due to a strong on-site Coulomb repulsion, which results in the semiconducting behavior of this compound.

One of the most important targets in recent research in the field of molecular solids is to produce an organic–inorganic hybrid system having multifunctionality coupled with transport, optical and magnetic properties. Multifunctional materials are expected to provide a unique interplay between these properties, such as a photo-tunable conductivity, field-induced superconductivity, or light controllable magnetism. For example, a metallic organic conductor coexisting with ferromagnetism $((BEDT\text{-}TTF)_3[Mn(II)Cr(III)(C_2O_4)_3])$ (BEDT-TTF: 4,5-bis(ethylenedithio)tetrathiafulvalene)) and a field-induced superconductor $(\lambda\text{-}(BETS)_2FeCl_4$ (BETS: 4,5-bis(ethylenedithio)tetraselenafulvalene)) have been reported.[1,2] In this way, hybrid molecular conductors containing functional counter ions will result in novel multifunctionality. Among them, radical cation salts based on BEDT-TTF are promising candidates for a molecular superconductor.[3]

Nitrosyl metal complexes, $[ML_n(NO)]$ (M = Fe, Ru, Os, L = ligand), which show persistent photo-induced metastable states at low temperature, have been intensively studied from the viewpoint of molecular devices.[4–6] Interestingly, the nitrosyl metal complexes show an inverted, or side-bound, NO ligand in their metastable state, which is coupled with an electronic excitation from the d_{xy} orbital of the metal to the π^* orbital of the NO ligand.[7] Although the metastable state is not a triplet, which was evidenced by ESR[8] and Mössbauer[9] measurements, the conduction band of the organic conductor may be affected when the nitrosyl complex in the organic conductor changes the coordination of the NO ligand by photoirradiation. If a nitrosyl metal complex is used as a counter anion for the BEDT-TTF salt, the multifunctional properties coupled with the transport and photochromic properties might be produced. In 1997, Zhu et al. reported a superconducting

transition at 7 K for $(BEDT\text{-}TTF)_4K[Fe(CN)_5NO]_2$.[10] Being stimulated by this report, radical cation salts of various organic donors with $[Fe(CN)_5NO]^{2-}$ and $[RuCl_5(NO)]^{2-}$ have been synthesized, which show various conducting behaviors, such as metallic, semiconducting, or insulating ones.[11–16] However, the superconductivity has not been reconfirmed. To explore light-controllable conducting materials, we synthesized a BEDT-TTF salt coupled with $[RuCl_5(NO)]^{2-}$. While Shevyakova et al. have reported on the crystallographic data and the semiconducting property of $\kappa\text{-}(BEDT\text{-}TTF)_4[RuBr_5(NO)]\cdot C_6H_5CN$ and reported $(BEDT\text{-}TTF)_4[RuCl_5(NO)]\cdot C_6H_5CN$ as an isostructural salt to $\kappa\text{-}(BEDT\text{-}TTF)_4[RuBr_5(NO)]\cdot C_6H_5CN$, no detailed crystallographic or magnetic property has been investigated for $(BEDT\text{-}TTF)_4[RuCl_5(NO)]\cdot C_6H_5CN$.[15] In this paper, we report on the crystallographic analysis and physical properties of $(BEDT\text{-}TTF)_4[RuCl_5(NO)]\cdot C_6H_5CN$. In addition, on the basis of structural and physical analyses, we clarified the intermolecular interaction and the partial electron transfer between BEDT-TTF and $[RuCl_5(NO)]$. A preliminary report of this compound has been communicated.[17]

Experimental

Reagents were of commercial grade. $(BEDT\text{-}TTF)_4[RuCl_5(NO)]\cdot C_6H_5CN$ was prepared by the electrical oxidation of BEDT-TTF (10 mg) in benzonitrile (18 mL) with $K_2[RuCl_5(NO)]$ (50 mg)(Soekawa Rika) and 18-crown-6 as supporting electrolytes. The oxidation of donor molecules was performed under a constant current of 0.5 μA in a conventional H-shaped cell at room temperature. After two weeks, single crystals were collected as shiny black thin plates with a typical size of ca. $1.0 \times 0.5 \times 0.1$ mm^3.

Table 1. Crystal Data for (BEDT-TTF)$_4$[RuCl$_5$(NO)]·C$_6$H$_5$CN at 298 K and 77 K

Empirical formula	C$_{47}$H$_{32}$S$_{32}$N$_2$ORuCl$_5$	C$_{47}$H$_{32}$S$_{32}$N$_2$ORuCl$_5$
Formula weight	1944.99	1944.99
Temperature	298 K	77 K
Wave length of X-ray	1.54180 Å	1.54180 Å
Crystal system	triclinic	triclinic
Space group	$P\bar{1}$	$P\bar{1}$
a	8.780(7) Å	8.672(6) Å
b	11.950(10) Å	11.737(9) Å
c	17.205(14) Å	17.045(12) Å
α	95.332(11)°	94.734(11)°
β	92.545(15)°	92.628(15)°
γ	95.135(14)°	95.035(13)°
V	1788(2) Å^3	1720(2) Å^3
Z	1	1
$F(000)$	977	977
Absorption coefficient	1.381 mm^{-1}	1.44 mm^{-1}
Collected reflections	14653	14296
Independent reflections	7856	7556
Parameters	416	416
R_1, $wR^{*a)}$	0.0934, 0.2555	0.0650, 0.1584

a) R factor definition: $R_1 = \Sigma(F_o - F_c)/\Sigma F_o$, wR factor definition: $wR = [\Sigma\{\omega(F_o^2 - F_c^2)^2\}/\Sigma[\omega(F_o^2)^2]]^{1/2}$, $\omega = 1/[\sigma(F_o^2) + (0.0890P)^2 + 0.00P]$ (for 298 K) and $\omega = 1/[\sigma(F_o^2) + (0.00P)^2 + 0.00P]$ (for 77 K), $P = (F_o^2 + 2F_c^2)/3$

X-ray diffraction data at 298 K and 77 K were collected with a RIGAKU AFC-8 Mercury CCD Automated X-ray Imaging System. A numerical absorption correction was carried out. The crystal structure was solved by a direct method with the SHELXS-97 program.[18] Full-matrix least-squares refinements were performed on F^2 against all reflections with the SHELXL-97 program.[18] The calculations were carried out with the WinGX package program.[19] The positions of the hydrogen atoms were calculated geometrically without any refinement. All of the atoms, except for hydrogen atoms, were refined anisotropically.

The tight-binding band calculation was carried out based on the extended Hückel method using the Slater-type orbitals (ζ) and the ionization potentials (ε) from Ref. 20. The intermolecular transfer integrals (t) were assumed to be proportional to the corresponding overlap integrals (S) of the HOMO of BEDT-TTF ($t = -ES$, $E = 10$ eV).

The electrical conductivities were measured by a conventional four-probe method, and an external pressure was applied using a clamp-type pressure cell. The pressure was monitored by the resistance of a Manganin wire. The magnetic susceptibility was measured using a Quantum Design MPMS5 SQUID susceptometer in the temperature range of 2–300 K. About 100 single crystals were stuck to the interior wall of a plastic straw by Apiezon N grease with the c-axis aligned parallel to an external magnetic field of 0.5 T. The Pascal diamagnetic contribution (-1.2×10^{-5} emu/mol) and an impurity Curie-tail of magnetic impurities (Curie constant of the impurity is 3.7×10^{-4} emu K/mol) were subtracted. The EPR spectra were measured by an X-band JES-TES300 spectrometer in the temperature range of 5–250 K. Raman spectroscopy was carried out in the backward geometry using a Renishaw Ramascope System 1000 with a He–Ne laser (632.8 nm) for excitation. The Raman spectra below 300 K were measured with a cryostat (Oxford Microstat HE). The single crystal, whose temperature was monitored with a silicon diode fixed in the sample stage, was mounted with Apiezon N grease.

Results and Discussion

Crystal Structure and the Oxidation State of BEDT-TTF. The crystallographic data for (BEDT-TTF)$_4$[RuCl$_5$(NO)]·C$_6$H$_5$CN at 298 K and 77 K are listed in Table 1.

As shown in Fig. 1(a), the crystal structure consists of alternating layers of BEDT-TTF cations and [RuCl$_5$(NO)]. The layers of [RuCl$_5$(NO)] contain solvent molecules, C$_6$H$_5$CN. Since an organic layer is formed by the dimers of BEDT-TTF molecules arranged almost perpendicular to each other (Fig. 1(b)), the donor arrangement of this compound belongs to the κ-type. One centrosymmetric pair of the BEDT-TTF (I) molecules is surrounded by four pairs of the crystallographically independent BEDT-TTF (II) molecules.

[RuCl$_5$(NO)] and C$_6$H$_5$CN are respectively located at the inversion center so that the NO ligand of [RuCl$_5$(NO)] and the CN group of benzonitrile are disordered over two positions. In general, the Ru–N–O angle, α, is a good indicator of the electronic state of the NO ligand, because a negative NO is bent ($\alpha = 120°$) and a positive NO is bonded linearly ($\alpha = 180°$) to the ruthenium atom.[21] In the title compound, α is 164° (Fig. 1(c)) and the valence state of the NO ligand in [RuCl$_5$(NO)] is considered to be an intermediate state between NO$^-$ and NO$^+$. As mentioned in the following EPR section, we can determine that ruthenium is divalent and diamagnetic, because no EPR signal assigned to Ru$^{+2+\delta}$ has been observed. Therefore, the electronic state in [RuCl$_5$(NO)] is expressed as [Ru^{2+}Cl$_5{}^{5-}$(NO)$^\delta$]$^{(\delta-3)}$ ($-1 < \delta < +1$).

CCDC256867 (for 298 K) and 256868 (for 77 K) contain the supplementary crystallographic data for this paper. These data can be obtained free of charge via www.ccdc.cam.ac.uk/data_request/cif, or by emailing data_request@ccdc.cam.ac.uk, or by contacting The Cambridge Crystallographic Data Centre, 12, Union Road, Cambridge CB2 1EZ, UK; fax: +44 1223.
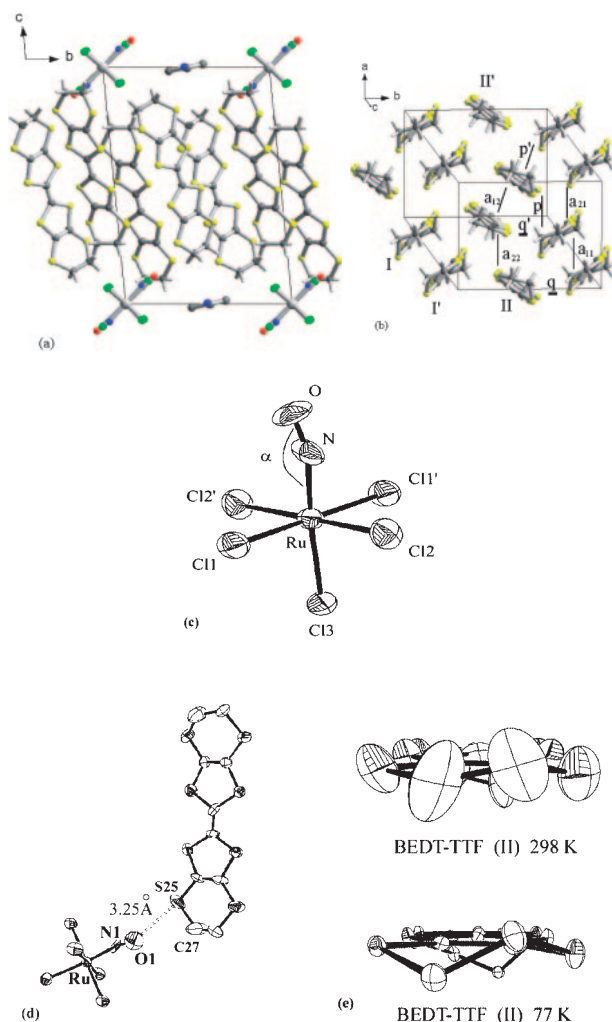
Fig. 1. (a) Projection of (BEDT-TTF)$_4$[RuCl$_5$(NO)]·
C$_6$H$_5$CN viewed along the *a*-axis. (b) The BEDT-TTF
cation layer: I and II, *x*, *y*, *z*, I′ and II′, $1-x$, $1-y$,
$1-z$. The inter-molecular interactions are also labeled.
The inter-molecular interaction energies for the band cal-
culations are as follows: $a_{11} = 132$, $a_{12} = 277$, $a_{21} = 126$,
$a_{22} = 122$, $p = 62$, $p′ = 0.5$, $q = 74$, and $q′ = 13$ meV.
(c) Projection of the anion; only one of the two possible
position of NO and Cl is indicated. (d) View of the short
intermolecular contact between the BEDT-TTF (II) mole-
cule and the NO ligand. (e) Projection view of the BEDT-
TTF (II) molecule at 298 K and 77 K along the long mo-
lecular axis. Hydrogen atoms are omitted for clarity.

As for the BEDT-TTF layer, it is important to determine the
oxidation state of BEDT-TTF molecules for the band calcula-
tion, because the oxidation state of BEDT-TTF molecules af-
fects the filling of the conduction band and the Fermi energy.
Raman spectroscopy is one of the most powerful techniques
for determining the oxidation state of the BEDT-TTF
molecules. Figure 2 shows the backward Raman spectrum
corresponding to the C=C stretching modes (ν_3 and ν_4) of
the BEDT-TTF molecule for (BEDT-TTF)$_4$[RuCl$_5$(NO)]·
C$_6$H$_5$CN at 298 K. The strong single peak at 1448 cm^{-1} cor-
responding to the ν_4 mode indicates that all of the BEDT-TTF
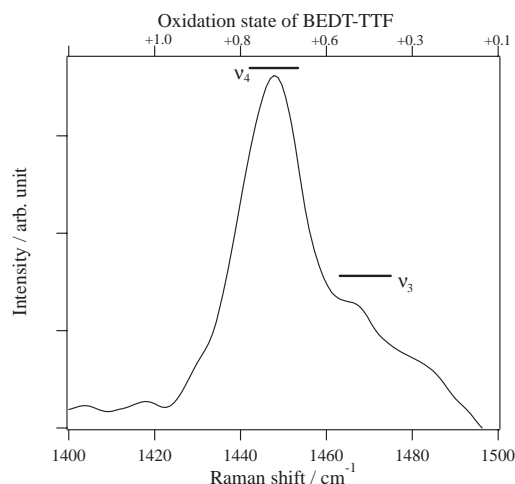molecules in (BEDT-TTF)$_4$[RuCl$_5$(NO)]·C$_6$H$_5$CN have the

Fig. 2. The Raman spectrum corresponding to the C=C
stretching modes (ν_3, ν_4) of the BEDT-TTF molecule
for (BEDT-TTF)$_4$[RuCl$_5$(NO)]·C$_6$H$_5$CN at 298 K. $\nu_4 =$
1450 cm^{-1} corresponds to the charge of +0.7.

same oxidation state. According to Wang et al.,[22] the oxidation
state (*Q*) of a BEDT-TTF molecule is estimated as,

$$Q = \frac{1508 - \nu_4}{88.4}. \tag{1}$$

Substituting $\nu_4 = 1448$ cm^{-1} in Eq. 1, *Q* is estimated at +0.7.
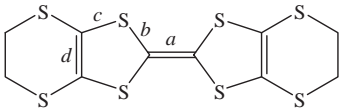The relationship between the oxidation state of the BEDT-
TTF molecule and the bond lengths within BEDT-TTF
molecules supports this result. Guionneau et al.[23] reported an
equation for determining the oxidation state of BEDT-TTF
molecule,

$$Q = 6.347 - 7.463\delta, \tag{2}$$

where $\delta = (b + c) - (a + d)$ and *a*, *b*, *c*, *d* are the averaged
bond lengths (see the definition in Table 2). The averaged bond
lengths, calculated parameters and oxidation states of BEDT-
TTF (I) and BEDT-TTF (II) as well as those of other BEDT-
TTF salts are listed in Table 2. Using Eq. 2, the oxidation
states of BEDT-TTF (I) and BEDT-TTF (II) are estimated at
+0.8 and +0.6, respectively. Taking account of the deviation
(± 0.1) between *Q* and the real charge, as shown in Table 2,
this result reasonably supports the oxidation state ($Q =$
+0.7) of BEDT-TTF molecules in the title compound, estimat-
ed from the Raman spectrum.

It should be noted that there is a short intermolecular contact
between the BEDT-TTF (II) molecule and the NO ligand, as
shown in Fig. 1(d) (S25–O1 = 3.26(3) Å), which is as short
as the sum of the corresponding van der Waals radii (3.25
Å). Through this pass, some interaction between the cationic
layer and the anionic layer is expected. Considering further
the overall charge neutrality in this compound, the charge
on each molecule is expressed as (BEDT-TTF$^{0.7+}$)$_4$-
[Ru^{2+}Cl$_5$$^{5-}(NO)^{0.2+}$]$^{2.8-}$. In other words, partial electron
transfer from the cationic layer of BEDT-TTF to the anionic
layer of [RuCl$_5$(NO)] through the short intermolecular contact
presumably takes place.

A similar partial electron transfer from the cationic layer
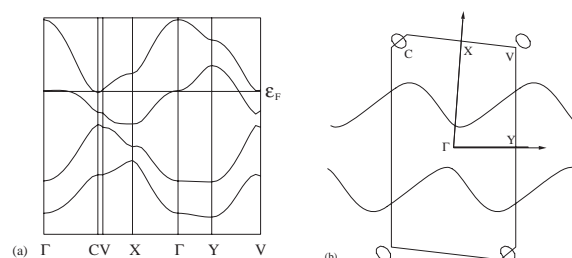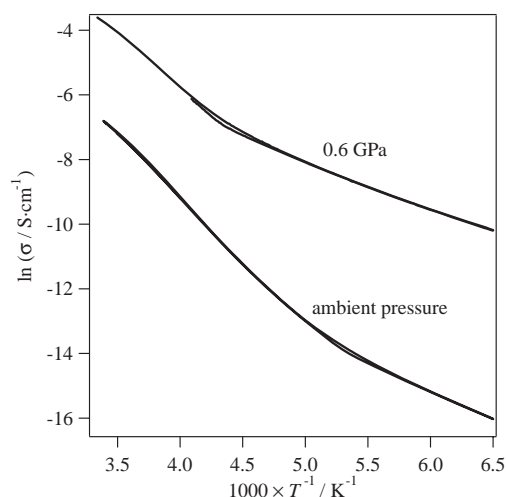to the anionic layer was reported in (BETS)$_2$[RuBr$_5$(NO)],[14]

Table 2. Averaged Bond Lengths (a, b, c, d), Calculated Parameters ($\delta = (b + c) - (a + d)$), Charges Q ($Q = 6.347 - 7.463\delta$) and Labeling of the C–S and C=C Averaged Bond Lengths

	BEDT-TTF	a (Å)	b (Å)	c (Å)	d (Å)	δ	Q	Real charge per BEDT-TTF	Ref.
(BEDT-TTF)$_4$[RuCl$_5$(NO)]C$_6$H$_5$CN	I	1.41	1.735	1.756	1.341	0.74	0.82	0.7	this work
	II	1.366	1.746	1.75	1.362	0.768	0.62	0.7	this work
Neutral BEDT-TTF		1.343	1.756	1.76	1.333	0.84	0.08	0	23
(BEDT-TTF)$_2$GaI$_4$	I	1.37	1.735	1.749	1.341	0.773	0.58	0.5	23
	II	1.373	1.732	1.748	1.33	0.777	0.55	0.5	23
(BEDT-TTF)$_2$Ge(C$_2$O$_4$)$_3$C$_6$H$_5$CN	I	1.404	1.716	1.742	1.35	0.704	1.09	1	24
	II	1.406	1.713	1.735	1.367	0.675	1.31	1	24

although the electronic state was reported as (BETS)$_2^{+2+\delta}$-[Ru$^{\delta+}$+Br$_5$(NO)]. In (BETS)$_2$[RuBr$_5$(NO)], the Ru–N–O angle, α (160°), and a large asymmetric EPR signal at $g = 2.037$ strongly suggest electron transfer, while there is no electron transfer in (BETS)$_2$[RuCl$_5$(NO)]. As can be seen from these examples, the substitution of the ligand dramatically affects the electron transfer. Similarly, the electronic state in (BEDT-TTF)$_4$[RuCl$_5$(NO)]·C$_6$H$_5$CN is clearly different from the case of κ-(BEDT-TTF)$_4$[RuBr$_5$(NO)]·C$_6$H$_5$CN, where there is no electron transfer ($\alpha = 180°$, NO$^+$, BEDT-TTF$^{0.5+}$ × 4).[15] According to Ref. 15, the intermolecular contact between the BEDT-TTF (II) molecule and the NO ligand in (BEDT-TTF)$_4$[RuCl$_5$(NO)]·C$_6$H$_5$CN is slightly shorter than that in κ-(BEDT-TTF)$_4$[RuBr$_5$(NO)]·C$_6$H$_5$CN (S(BEDT-TTF)–O(NO) = 3.32 Å). Therefore, we can simply hypothesize that the shorter contact in (BEDT-TTF)$_4$-[RuCl$_5$(NO)]·C$_6$H$_5$CN induces partial electron transfer from the BEDT-TTF molecule to the NO ligand. However, the intermolecular contact between the BETS molecule and the NO ligand in (BETS)$_2$[RuBr$_5$(NO)] (Se(BETS)–O(NO) = 3.672(15) Å) is much longer than that of (BETS)$_2$[RuCl$_5$(NO)] (Se(BETS)–O(NO) = 3.293(24) Å). The overlap between the HOMO of BEDT-TTF and the π^* orbital of the NO ligand is presumably important for the electron-transfer mechanism.

To investigate the electronic structure, we carried out a tight-binding band calculation based on an extended Hückel method. Calculations without the Coulomb repulsion were carried out for (BEDT-TTF$^{0.7+}$)$_4$. The band structure and the Fermi surfaces at 298 K are shown in Figs. 3(a) and 3(b), respectively. The Fermi surfaces consist of the major open Fermi surface and the minor closed one. The existence of the Fermi surface suggests a metallic behavior for this compound.

Physical Properties of (BEDT-TTF)$_4$[RuCl$_5$(NO)]·C$_6$H$_5$CN. The temperature dependence of the electrical conductivity under ambient pressure is plotted in Fig. 4. As shown in Fig. 4, (BEDT-TTF)$_4$[RuCl$_5$(NO)]·C$_6$H$_5$CN behaves as a semiconductor with a conductivity of $\sigma \sim 10^{-3}$ S/cm at room temperature and the activation energy (Δ) of 4500 K. Below the critical temperature (T_c) where a phase transition occurs with thermal hysteresis (around 180 K), an activation energy becomes $\Delta = 1500$ K. The semiconducting behavior is re-

Fig. 3. (a) Band structure and (b) Fermi surface for (BEDT-TTF)$_4$[RuCl$_5$(NO)]·C$_6$H$_5$CN at 298 K.

Fig. 4. Logarithmic plots of the conductivity vs $1000/T$ for (BEDT-TTF)$_4$[RuCl$_5$(NO)]·C$_6$H$_5$CN under ambient pressure and 0.6 GPa.

tained under pressure up to 0.6 GPa ($\sigma \sim 10^{-1}$ S/cm at room temperature, $\Delta = 1500$ K), while T_c increases ($T_c = 240$ K, $\Delta(T < T_c) = 400$ K). To reveal the origin of the phase transition at 180 K, we carried out an X-ray crystallographic analysis at 77 K. Compared with the crystal structure at room temperature, the carbon atoms in the ethylene groups with large thermal factors at room temperature were refined into distinct sites with small thermal factors (Fig. 1(e)). Since this result indicates that the disorder in the ethylene groups of the BEDT-
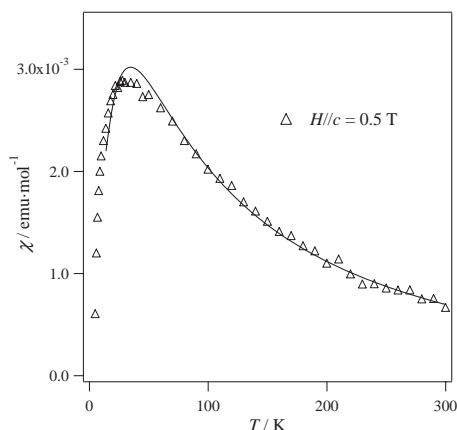
Fig. 5.   Temperature dependence of the magnetic suscepti-
bility for $(BEDT\text{-}TTF)_4[RuCl_5(NO)]\cdot C_6H_5CN$ with the
magnetic field parallel to the *c*-axis. The solid curve is
the fitting to the two-dimensional square-lattice $S = 1/2$
Heisenberg antiferromagnet with $J/k_B = -23$ K.

TTF molecules disappears at 77 K, the phase transition at 180
K is attributed to the order–disorder transition in the ethylene
groups of the BEDT-TTF molecules.

The semiconducting behavior is contrary to the expectation
from a band calculation. This contradiction indicates that the
effective on-site Coulomb repulsion, which is not considered
in the band calculation, is important in this system.

To estimate the magnitude of the effective on-site Coulomb
repulsion, magnetic susceptibility measurements were carried
out. Figure 5 shows the temperature dependence of the mag-
netic susceptibility with the applied field parallel to the *c*-axis.
Similar results were obtained from measurements with the
field parallel to the *a*- and *b*-axes. Using the χ value at room
temperature, the effective moment, μ_{eff}, is estimated at 1.55
μ_B. This value falls within the range of the expected value
for one spin with $S = 1/2$ in the unit cell, which is too small
for $(BEDT\text{-}TTF)_4{}^{2+}$, but appropriate for $(BEDT\text{-}TTF)_4{}^{2.8+}$.

In the Hubbard model, the magnetic susceptibility, χ_{spin}, is
expressed as,

$$\chi_{spin} = \frac{2\mu_B{}^2 N_F}{(1 - U_{eff} \times N_F)}, \qquad (3)$$

where U_{eff} is the effective on-site Coulomb repulsion and N_F is
the density of states at the Fermi level. Equation 3 represents
the enhancement of the magnetic susceptibility by an effective
on-site Coulomb repulsion. For instance, typical metallic
BEDT-TTF salts have a small magnetic susceptibility ($\chi =
5 \times 10^{-4}$ emu/mol at room temperature),[25] while a Mott insu-
lator, $\alpha'\text{-}(BEDT\text{-}TTF)_2AuBr_2$, has a magnetic susceptibility
comparable to the title compound ($\chi = 10^{-3}$ emu/mol at room
temperature).[26] Moreover, the temperature dependence of the
magnetic susceptibility for a low-dimensional antiferromag-
netic spin system with strong on-site Coulomb repulsion shows
a broad maximum. In fact, the title compound shows a broad
maximum in χ as a function of the temperature (around 40
K). These results suggest that the title compound is situated
at the localized spin system.[27]

Generally, organic charge transfer salts based on BEDT-
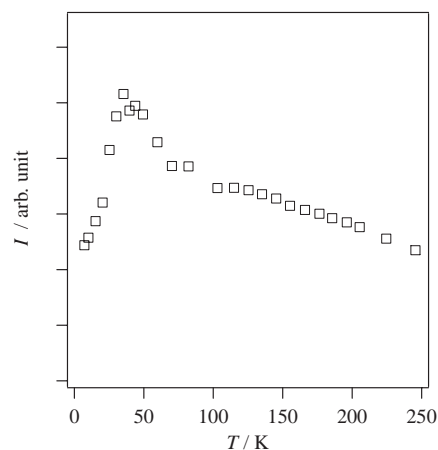TTF, especially κ-type salts, are two-dimensional conductors.

Fig. 6.   Temperature dependence of the EPR intensity for
$(BEDT\text{-}TTF)_4[RuCl_5(NO)]\cdot C_6H_5CN$.

Therefore, we fitted the temperature dependence of the mag-
netic susceptibility for a two-dimensional Heisenberg antifer-
romagnet.[28] The solid line in Fig. 5 is the calculated suscepti-
bility with an exchange interaction of $J = -23$ K. The calcu-
lation was carried out in the temperature range between 300 K
and 20 K (above $T = 0.9JS(S + 1)$) because of the limitation
of the high-temperature series expansion method. Since this
two-dimensional model completely reproduces the experimen-
tal values, all charges are localized at the BEDT-TTF mole-
cules.

An EPR measurement also confirms the electronic structure
of this salt. At room temperature, we can observe one EPR sig-
nal with Lorentzian resonance curve ($\Delta H_{peak\text{–}peak} = 6.8$ mT,
$g = 2.009$ ($H \parallel b$)), which is due to the BEDT-TTF radicals.
Figure 6 shows the temperature dependence of the EPR inten-
sity in the magnetic field parallel to the *c*-axis. The EPR inten-
sity, which is proportional to χ_{spin}, reproduces the temperature
dependence of the magnetic susceptibility. This result supports
the localized model. Therefore, the semiconducting behavior
in this compound can be explained by the localized model
due to the strong on-site Coulomb repulsion.

The Mott insulator has a band gap (E_g), since the effective
on-site Coulomb repulsion (U_{eff}) is larger than the Hubbard
sub-band width (W) due to the strong intra-dimer correlation
(t_{intra}) and the weak inter-dimer correlation (t_{inter}). However,
even if there is a band gap between the upper Hubbard sub-
band and the lower Hubbard one, this compound has carriers
in the lower Hubbard sub-band due to a partial electron trans-
fer from BEDT-TTF to $[RuCl_5(NO)]$. This is contrary to the
experimental results. Most likely, a small amount of charge
separation in the BEDT-TTF layer, which cannot be distin-
guished by Raman spectroscopy, may generate a new band
gap in the lower Hubbard sub-band, which results in the semi-
conducting behavior. In order to investigate this hypothesis,
more detailed structural analyses using a synchrotron powder
diffraction experiment and MEM/Rietveld analysis are in
progress.

Interestingly, a residual three-line spectrum ($g = 2.005$,
$A = 0.8$ mT), which is similar to that observed for $[Fe^{2+}\text{-}
(CN)_5{}^{5-}(NO)^\delta]^{\delta-3}$ ($g = 1.98$, $A = 1.8$ mT),[8] is recorded be-
low 20 K after subtraction of the EPR signal of the BEDT-
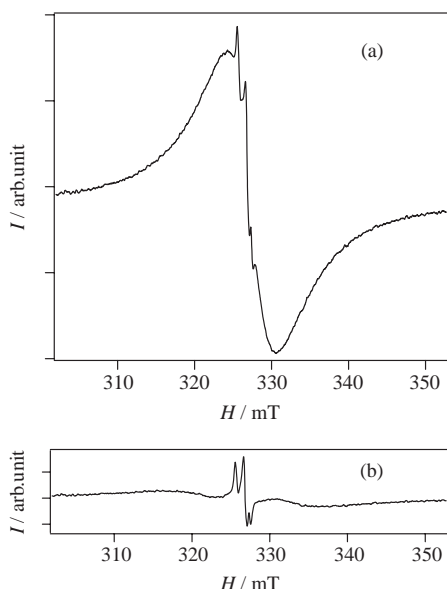
Fig. 7. (a) EPR spectra of $(BEDT\text{-}TTF)_4[RuCl_5(NO)]\cdot$ C_6H_5CN at 10 K with the field parallel to the *a* axis. (b) The residual three-line spectra due to a spin coupled with a ^{14}N nucleus ($I = 1$).

TTF radical (Fig. 7(b)). The residual spectrum having three branches can be interpreted in the same manner of $[Fe^{2+}\text{-}(CN)_5{}^{5-}(NO)^\delta]^{\delta-3}$, where an effective spin ($S = 1/2$) in the π^* orbital of the NO ligand exhibits a hyperfine splitting due to the coupling of an unpaired electron with a ^{14}N nucleus ($I = 1$). This result indicates the existence of an unpaired electron in the π^* orbital of the NO ligand, and confirms partial electron transfer from the BEDT-TTF molecule to the NO ligand in $[RuCl_5(NO)]$.

In order to investigate the existence of the metastable state in the ruthenium complex, Raman spectra were measured at 100 K before and after the light irradiation (Ar^+ laser, 514.5 nm). Generally, nitrosyl complexes generate metastable states through the MLCT (metal-to-ligand charge transfer), and a new Raman spectrum should be observed after the generation of the metastable state.[29] However, in this compound, no spectral change was induced by the light irradiation, and hence the metastable state of $[RuCl_5(NO)]$ could not be detected. The electron, which is transferred from the BEDT-TTF layer to the NO ligand in $[RuCl_5(NO)]$, might prevent the initial excitation (MLCT) from taking place.

Another possible reason for the absence of the metastable state for $[RuCl_5(NO)]$ may be the low thermal stability due to the interaction between the ruthenium complex and BEDT-TTF. In fact, the metastable state of $[FeCN_5(NO)]$ in $(BEDT\text{-}TTF)_4K[Fe(CN)_5(NO)]$ is less stable than that of $Na_2[Fe(CN)_5(NO)]$.[30]

Conclusion

We investigated the crystal structure and the physical properties of $(BEDT\text{-}TTF)_4[RuCl_5(NO)]\cdot C_6H_5CN$. Based on an X-ray crystallographic analysis, the donor arrangement of this compound belongs to the κ-type. X-ray crystallographic data, EPR and Raman spectra proved that the partial electron, transferred from the BEDT-TTF layer through the short intermo-

lecular contact, occupies the π^* orbital of the NO ligand in $[RuCl_5(NO)]$. Raman spectroscopy determined the oxidation state of the BEDT-TTF molecules in $(BEDT\text{-}TTF)_4[RuCl_5(NO)]\cdot C_6H_5CN$ as $+0.7$. The band calculation, magnetic susceptibility and EPR measurements revealed that this compound is situated at the localized spin system due to a strong on-site Coulomb repulsion. The strong on-site Coulomb repulsion prevents charge delocalization, which results in the semiconducting behavior. The magnetic susceptibility measurement also revealed that the title compound behaves as a two-dimensional Heisenberg antiferromagnet with $J = -23$ K. However, even if there is the band gap between the upper Hubbard sub-band and the lower one due to the strong on-site Coulomb interaction, this compound has carriers in the lower Hubbard sub-band due to partial electron transfer from BEDT-TTF to $[RuCl_5(NO)]$. In order to clarify this problem, more detailed structural analyses using synchrotron X-ray diffraction and MEM/Rietveld analysis are in progress.

This work revealed a unique interplay between BEDT-TTF and the nitrosyl ruthenium complex, which results in a partial electron transfer from the cationic layer to the anionic layer. If we can control the partial electron transfer between the NO ligand in $[RuCl_5(NO)]$ and the BEDT-TTF layer by photo-irradiation, it would be possible to produce a photo-controllable conductor.

References

1   E. Coronado, J. R. Galán-Mascarós, C. J. Gómez-García, and V. Laukhin, *Nature*, **408**, 447 (2000).

2   S. Uji, H. Shinagawa, T. Terashima, T. Yakabe, Y. Terai, M. Tokumoto, A. Kobayashi, H. Tanaka, and H. Kobayashi, *Nature*, **410**, 908 (2001).

3   T. Ishiguro, K. Yamaji, and G. Saito, "Organic Superconductors," 2nd ed, Springer-Verlag, Berlin (1998).

4   Th. Woike, W. Krasser, P. Bechthold, and S. Haussühl, *Phys. Rev. Lett.*, **53**, 1767 (1984).

5   M. D. Carducci, M. R. Pressprich, and P. Coppens, *J. Am. Chem. Soc.*, **119**, 2669 (1997).

6   C. Kim, I. Novozhilova, M. S. Goodman, K. A. Bagley, and P. Coppens, *Inorg. Chem.*, **39**, 5791 (2000).

7   P. Coppens, D. V. Formitchev, M. D. Carducci, and K. Culp, *J. Chem. Soc., Dalton Trans.*, **1998**, 865.

8   C. Terrile, O. R. Nascimento, I. J. Moraes, E. E. Castellano, O. E. Piro, J. A. Guida, and P. J. Aymonino, *Solid*

State Commun., **73**, 481 (1990).

9   Th. Woike, W. Kirchner, H. Kim, S. Haussühl, V. Rusanov, V. Angelov, S. Ormandjiev, Ts. Bonchev, and A. N. F. Schroeder, *Hyperfine Interact.*, **77**, 265 (1993).

10   H. Yu and D. Zhu, *Physica C*, **282–287**, 1893 (1997).

11   L. Kushch, L. Buravov, V. Tkacheva, E. Yagubskii, L. Zorina, S. Khasanov, and R. Shibaeva, *Synth. Met.*, **102**, 1646 (1999).

12   M. Clemente-León, E. Coronado, J. R. Galán-Mascarós, C. J. Gómez-García, and E. Canadell, *Inorg. Chem.*, **39**, 5394 (2000).

13   L. V. Zorina, S. S. Khasanov, R. P. Shibaeva, M. Gener, R. Rousseau, E. Canadell, L. A. Kushch, E. B. Yagubskii, O. O. Drozdova, and K. Yakushi, *J. Mater. Chem.*, **9**, 2017 (2000).

14   M. E. Sanchez, M. L. Doublet, C. Faulmann, I. Malfant, P. Cassoux, L. A. Kushch, and E. B. Yagubskii, *Eur. J. Inorg. Chem.*, **2001**, 2797.

15   I. Y. Shevyakova, L. V. Zorina, S. S. Khasanov, L. I. Buravov, V. A. Tkacheva, R. P. Shibaeva, E. B. Yagubskii, and E. Canadell, *J. Solid State Chem.*, **168**, 514 (2002).

16   I. Y. Shevyakova, L. I. Buravov, L. A. Kushch, E. B. Yagubskii, S. S. Khasanov, L. V. Zorina, R. P. Shibaeva, N. V. Drichko, and I. Oleinischak, *Russ. J. Coord. Chem.*, **28**, 487 (2002).

17   M. Okubo, T. Komatsu, N. Matsushita, N. Kojima, and G. Saito, *Mol. Cryst. Liq. Cryst.*, **376**, 147 (2002).

18   G. M. Sheldrick, "SHELX97: Program for Crystal Structure Analysis," Institute für Anorganische Chemie der Universität, Tammanstrasse 4, D-3400 Göttingen, Germany (1998).

19   WinGX: L. J. Farrugia, *J. Appl. Cryst.*, **32**, 837 (1999).

20   T. Mori, A. Kobayashi, Y. Sasaki, H. Kobayashi, G. Saito, and H. Inokuchi, *Bull. Chem. Soc. Jpn.*, **57**, 627 (1984).

21   M. Ogasawara, D. Huang, W. E. Streib, J. C. Huffmann, N. Gallego-Planas, F. Maseras, O. Eisenstein, and K. G. Caulton, *J. Am. Chem. Soc.*, **119**, 8642 (1997).

22   H. H. Wang, J. R. Ferraro, J. M. Williams, U. Geiser, and J. A. Schlueter, *J. Chem. Soc., Chem. Commun.*, **1994**, 1893.

23   P. Guionneau, C. J. Kepert, G. Bravic, D. Chasseau, M. R. Truter, M. Kurmoo, and P. Day, *Synth. Met.*, **86**, 1973 (1997).

24   L. Martin, S. S. Turner, P. Day, P. Guionneau, J. A. K. Howard, M. Uruichi, and K. Yakushi, *J. Mater. Chem.*, **9**, 2731 (1999).

25   H. Urayama, H. Yamochi, G. Saito, K. Nozawa, T. Sugano, M. Kinoshita, S. Sato, K. Oshima, A. Kawamoto, and J. Tanaka, *Chem. Lett.*, **1988**, 55.

26   S. D. Obertelli, R. H. Friend, D. R. Talham, M. Kurmoo, and P. Day, *J. Phys., Condens. Matter*, **1**, 5671 (1989).

27   N. Yoneyama, A. Miyazaki, T. Enoki, and G. Saito, *Bull. Chem. Soc. Jpn.*, **72**, 639 (1999).

28   G. S. Rushbrooke and P. J. Wood, *Mol. Phys.*, **1**, 257 (1958).

29   Th. Woike, H. Zöllner, W. Krasser, and S. Haussühl, *Solid State Commun.*, **73**, 149 (1990).

30   S. V. Kapelnitsky, E. B. Yagubskii, L. A. Kushch, and I. Y. Shevyakova, *JETP Lett.*, **76**, 165 (2002).